
Article:
Evans, RML orcid.org/0000-0003-4172-8455, Hall, CA, Aditi Simha, R et al. (1 more author) (2015) Classical XY model with conserved angular momentum is an archetypal non-Newtonian fluid. Physical Review Letters, 114. 138301. ISSN 0031-9007

https://doi.org/10.1103/PhysRevLett.114.138301

The classical XY model with conserved angular momentum is an archetypal non-Newtonian fluid

R. M. L. Evans*,[1] Craig A. Hall,[1] R. Aditi Simha,[2] and Tom S. Welsh
[1]*School of Mathematics, University of Leeds, LS2 9JT, United Kingdom*
[2]*IIT Madras*
(Dated: March 3, 2015)

We find that the classical one-dimensional (1D) XY model, with angular-momentum-conserving Langevin dynamics, mimics the non-Newtonian flow regimes characteristic of soft matter when subjected to counter-rotating boundaries. An elaborate steady-state phase diagram has continuous and first-order transitions between states of uniform flow, shear-banding, solid-fluid coexistence and slip-planes. Results of numerically studies and a concise mean-field constitutive relation, offer a paradigm for diverse non-equilibrium complex fluids.

Apart from the Ising model, the classical XY Model (also known as the classical rotor model or $O(2)$ model) is the simplest paradigm of condensed matter physics [1]. Like the Ising model, its applications extend far beyond the simple magnetic systems that first inspired it [2–4].

The 1D XY model consists of a chain of rotors (or "spins"), each with one continuous degree of freedom: the angle θ_j of a two-component unit vector $\mathbf{s}_j = (\cos\theta_j, \sin\theta_j)$. Each site couples only to its two nearest neighbours, via a potential that favours parallel alignment. So the Hamiltonian (in units of the coupling constant) is given by $H = \sum_{j=1}^{N}\left[-\mathbf{s}_j\cdot\mathbf{s}_{j-1} + \frac{1}{2}\dot\theta_j^2\right]$ where the rotor's moment of inertia (scaling the final, kinetic energy term) has been set to unity without loss of generality. As with any 1D system with short-range interactions, the 1D XY model has trivial equilibrium phase behaviour, with a single transition to an ordered state at zero temperature [5]. Away from equilibrium, we have found that this simple 1D model has an elaborate steady-state phase diagram with transitions between flow-regimes that mimic the phenomenology of soft matter [6, 7].

Whereas a Newtonian fluid, under uniform stress, flows with uniform shear rate, complex fluids (e.g. foams, particulate suspensions and smectic liquid crystals) can exhibit coexistence of macroscopic regions with distinct shear rates [8–15]. This phenomenon, known as shear banding, has been explained in terms of various models with non-trivial stress fields [16–19]. The definition of shear flow requires at least two spatial dimensions. In the 1D XY model, if we represent the unit vectors $\mathbf{s}_j$ lying in a plane perpendicular to the one spatial dimension of their locations j, then we can interpret their rotational velocity differences as shear rates. Surprisingly, we find the 1D XY model exhibits shear-banding and other non-Newtonian phenomena routinely seen in soft matter.

While equilibrium phase behaviour is independent of the model's dynamics, non-equilibrium states require us to specify an equation of motion. We use Langevin dynamics, at temperature T, with $k_B \equiv 1$, and include only forces (torques) that respect Newton's (rotational) third law of motion and so conserve angular momentum. So, like the conservative forces, the frictional and stochastic forces act only between neighbours, and depend on their relative motion and orientation. With only angular degrees of freedom — no radial motion — no centrifugal or coriolis forces act, so the system is independent of absolute angular velocity and respects an angular version of Galilean relativity. Thus the Langevin equation for the XY model with conserved angular momentum is given by

$$\ddot\theta_j = \tau_j - \tau_{j-1}, \tag{1}$$

$$\tau_j = \sin\Delta\theta_j + \mu\Delta\dot\theta_j + \eta_j(t) \tag{2}$$

where τ_j is the torque applied by rotor $j+1$ to rotor j, at relative angle $\Delta\theta_j = \theta_{j+1} - \theta_j$. The coefficient of friction is μ, and $\eta_j(t)$ are the usual delta-correlated Gaussian-distributed functions with $\langle\eta_i(t)\eta_j(t')\rangle = 2\mu T\delta(t-t')\delta_{ij}$ and zero mean. Hamilton's equations are recovered in the conservative case $T = \mu = 0$.

Although the model is insensitive to absolute rotational velocities, we can drive it into a non-equilibrium steady state by rotating one of its boundaries relative to the other (as in a parallel-plate rheometer shearing a sample of fluid [20–22]). To impose periodic boundary conditions whilst also applying a relative torque across the system, rotors at opposite ends of the chain are designated as neighbours, but see each other through an angular offset that increases at a constant angular velocity. Thus the set of N rotors lives in a periodic space with an overall twist that rotates at a rate $N\dot\gamma$. So all rotors respect the same equations of motion, and the Hamiltonian remains that of the XY model, while the system as a whole experiences a mean shear rate (angular velocity difference per rotor) of $\dot\gamma$.

Here, we present the results of numerically exploring the XY model's steady-state behaviour in shear flow, and a mean-field analysis explaining its phenomenology.

The DPD algorithm [23] was used to evolve the state of the system. Finite-size effects were eliminated by using $512 \le N \le 2048$. Statistically steady states were established by comparing systems with disparate initial conditions. The discrete time step dt was chosen adaptively to

*corresponding author mike.evans@physics.org

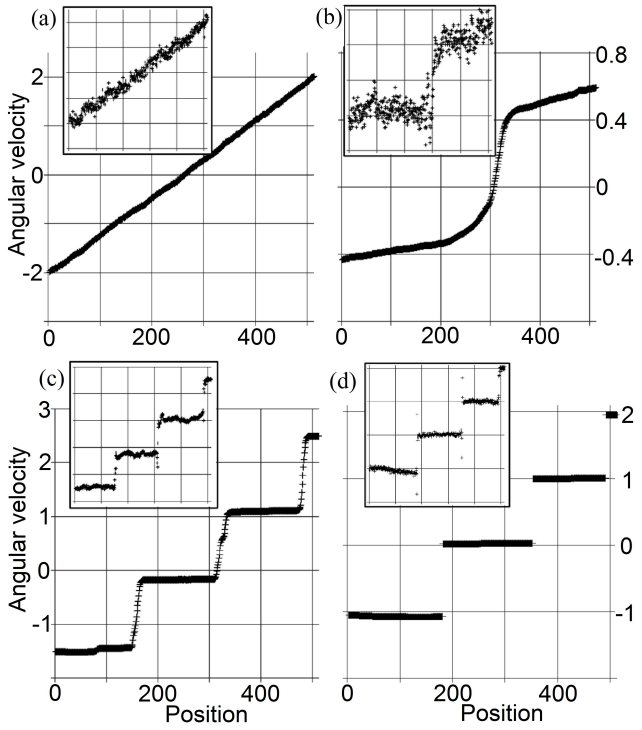

FIG. 1: Angular velocity *versus* position in a chain of 512 rotors, typifying the four distinct steady states at asymptotically late times ($t \geq 4500$). Main panels: time-averaged over several rotation-times ($\sim \dot{\gamma}^{-1}$). Insets: instantaneous snap-shots. (a) Uniform at $(T, \mu, \dot{\gamma}) = (0.02, 10, 0.007813)$; (b) shear banding at $(T, \mu, \dot{\gamma}) = (0.006, 1, 0.002)$. (c) solid-fluid coexistence at $(T, \mu, \dot{\gamma}) = (0.001, 1, 0.0078125)$; (d) Slip planes at $(T, \mu, \dot{\gamma}) = (0.001, 0.5, 0.00585938)$;

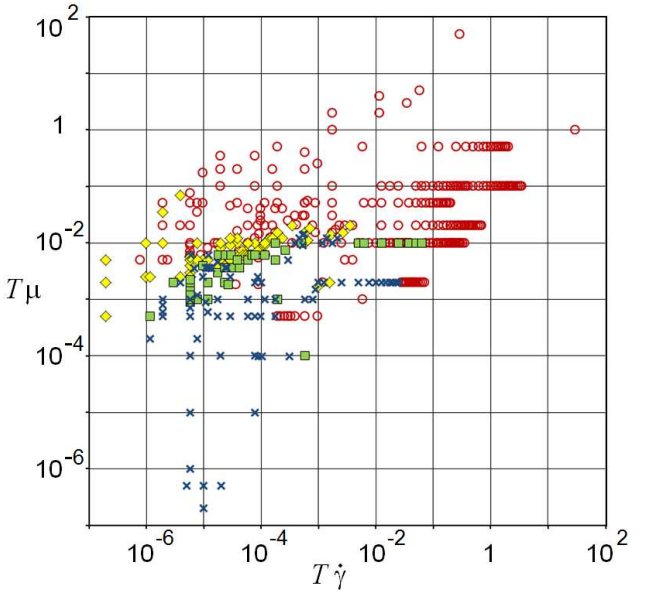

FIG. 2: (Colour on-line) Steady states, on axes $T\mu$ versus $T\dot{\gamma}$. Symbols represent: uniform phase (red open circles); shear banding (yellow filled diamonds); solid-fluid coexistence (green filled squares); slip-plane phase (blue crosses).

ensure that the relative angular increment between any neighbours never exceeded 0.2.

Four qualitatively distinct types of flow behaviour were observed (Fig. 1), separated by phase transitions or narrow cross-over regimes: a state of statistically uniform shear flow throughout the system, a shear-banding regime, a coexistence between solid and fluid regions, and a regime of solid regions separated by localized slip planes. Animations are available online [24].

Empirically, we find an approximate data-collapse (Fig. 2) into fairly clearly-defined phase regions on axes of $(T\dot{\gamma})$ and $(T\mu)$, allowing us to present all of our simulated phase data in one figure. The simulations were performed at values of μ ranging from 10^{-3} to 10^{2} and $\dot{\gamma}$ from 10^{-3} to 7.0. On increasing temperature or friction coefficient or shear rate, the trend is to progress from the slip-plane regime, through solid-fluid coexistence, then the shear-banding regime, to a uniform state. For some parameter values, one or both of the intermediate states are bypassed.

In the uniform phase, local shear rate $s_j \equiv \langle \mathrm{d}\Delta\theta_j/\mathrm{d}t \rangle$ is independent of location j, where $\langle \ldots \rangle$ indicates a time-average. Local shear rate s_j should not be confused with its spatial average, the global shear rate $\dot{\gamma}$. The two are equal in the uniform phase only. It exists at large parameter values, when either thermal energy or shear-induced kinetic energy of relative motion dominates over the interaction potential, or when frictional forces dominate over the potential gradient.

In the slip-plane regime, $s_j = 0$ at most locations j, and the relative angle $\Delta\theta_j$ exhibits only small-amplitude excursions about a constant value, within the potential well. These rotor-pairs are "locked" in the terminology of Büttiker et al. [25]. So, most of the system behaves as an elastic solid, while all of the shear flux is concentrated in a small population of isolated inter-rotor gaps (the slip planes), where the relative angle is "running". The location k of each slip plane remains fixed for a duration far exceeding its internal rotation time $2\pi/\Delta\dot{\theta}_k$. Slip planes in surfactant cubic phases have been modelled by Jones and McLeish [26] using the same periodic potential, treated perturbatively.

The stability of each solid region requires the time-averaged torque to be less than the largest potential gradient (unity), the threshold torque at which an elastic solid region would yield. This follows from time-averaging Eq. 2 given $s_j = 0$ by definition of "solid". Repeated traversing of the periodic potential at each slip plane creates a torque oscillation that propagates through the nearby solid as damped torsion waves, visible as very short slanting lines in Fig. 3a, which is a space-time diagram of the system's motion, with all of the shear concentrated in a single slip plane near the right-hand end. Meanwhile long wavelength torsional waves of lower amplitude travel across the entire system, visible

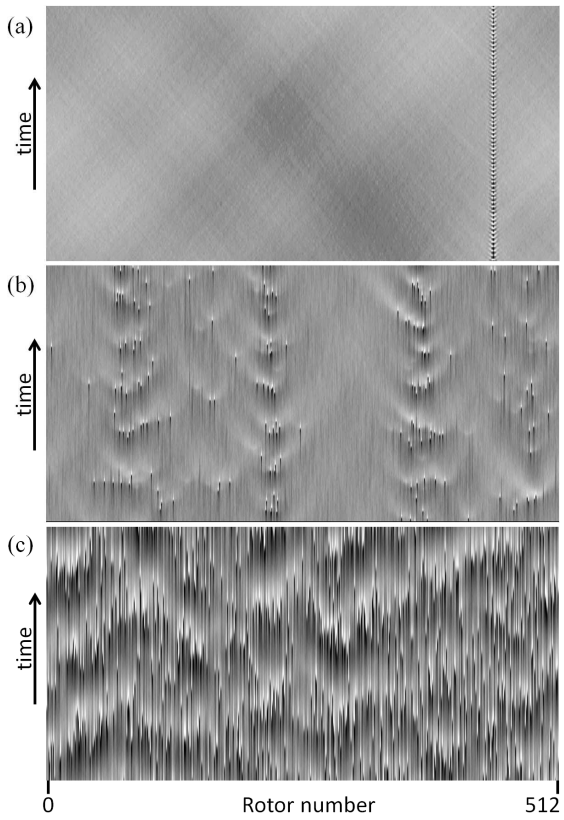

FIG. 3: Grey scale represents inter-rotor potential (from $U = -1$ (white) to $U = 1$ (black)) as a function of position (whole system shown horizonally) and time (increasing upwards). (a) At $(T, \mu, \dot{\gamma}) = (10^{-4}, 0.5, 0.001896)$, with one slip plane. Image spans 512 rotors and 375 time units, after initialization exceeding 4500 time units. (b) Solid-fluid coexistence at $(T, \mu, \dot{\gamma}) = (0.0005, 5, 0.002)$, showing $N = 1024$ rotors and 750 time units, after $t = 4500$. (c) At $(T, \mu, \dot{\gamma}) = (10^{-3}, 10, 0.017578125)$, a near-critical phase. Image spans $N = 1024$ rotors and 375 time units, after $t > 65000$.

as long, faint slanting marks in Fig. 3a.

Whereas the space-time diagram for slip planes (Fig. 3a) shows linear propagation of small-amplitude waves through the solid, large-amplitude non-linear waves of yielding events propagate through the fluid region of a solid-fluid coexistence (Fig. 3b), where black marks signify the maximum of the potential being overcome. Each yield event locally displaces enough stress to trigger another yield event nearby, creating slanting chains of events in Fig. 3b. Local stress excitations from these events maintain fluid activity within a finite region of the system, while the remaining portion can remain solid because the mean torque is just below the yield-point value (unity). Due to finite temperature, some relatively rare yield events occur in the "solid" region also, so that it is in fact a high-viscosity fluid, and this coexistence may not be qualitatively distinct from shear-banding.

It is surprising that the correlated chains of yield events persistently recur within the same finite locales (the fluid regions), rather than spreading across the whole system. We infer that there exists a threshold rate-density of barrier crossings, below which they cannot trigger each other in a chain reaction (though it is not obvious to us *why* it should exist). Thus, if the fluid region were to grow, at the expense of the solid, its local shear rate s_j would fall, since the global rate $\dot{\gamma}$ would be spread over a larger fluid. Thus the rate-density of barrier crossings within the fluid would drop below the threshold, causing a portion of it to re-freeze. If the fluid region were to shrink, its local shear rate would rise, causing mean torque to rise, due to the frictional term $\mu\Delta\dot{\theta}_j$ in Eq. 2. So part of the solid region would yield and melt. Thus the solid-fluid coexistence is maintained.

In the shear-banding regime, the system self-organises into macroscopic regions with different effective viscosities. A continuous transition appears to separate the shear-banded and uniform states, but we have not established whether this is an isolated critical point, a critical end-point of a first-order phase transition, or a line of continuous transitions. Near the transition, critical phenomena are observed. Although diverging correlation lengths are impossible in locally-interacting 1D systems at equilibrium, our non-equilibrium steady state exhibits correlated configurations (where $\Delta\theta \approx \pi \;\Rightarrow\; U \approx 1$) extending across large distances, but not at constant time, apparent only in the space-time domain (Fig. 3c). We note a resemblance to some of the flow phenomena in the space-time diagrams of Ref. [28].

The equation of motion (from Eq. (1)) for the relative angle $\Delta\theta_j$ between neighbours,

$$\Delta\ddot{\theta}_j = \tau_{j+1} + \tau_{j-1} - 2\tau_j, \tag{3}$$

with Eq. (2), forms a closed set of equations independent of any absolute angular positions θ_j. Imposing the steady-state condition that time-averaged accelerations vanish, together with the periodic boundary condition, that the torques are equal at opposite ends of the chain, Eq. (3) implies that time-averaged torque is uniform, $\langle\tau_j\rangle = \overline{\tau} \quad \forall\; j$, resembling a uniform-stress condition for steady shear flow of a fluid.

The equations of motion (3 and 2) are non-linear in $\Delta\theta_j(t)$ which is generally not a small variable. It is useful to recast them [27] in terms of the fluctuations $\varepsilon_j(t)$ about constant shear rate, defined (with vanishing time-average) by $\Delta\theta_j(t) = s_j\, t + c_j + \varepsilon_j(t)$ with constant offsets c_j. Time-averaging and using the boundedness of $\varepsilon_j(t)$ yields a relationship between local shear rate s_j and mean torque, $\overline{\tau} = \mu s_j + \big\langle \sin\big(s_j\, t + c_j + \varepsilon_j(t)\big)\big\rangle$. The final term would vanish for constant relative motion ($\varepsilon_j = 0$), yielding a Newtonian fluid of viscosity μ. But fluctuations at a frequency matching the local shear rate lead to a non-uniform distribution of angles $\Delta\theta_j$ and hence non-Newtonian rheology.

Next, we expand $\varepsilon_j(t)$ in Fourier modes, $\varepsilon_j(t) = \sum_\omega \hat{\varepsilon}_j(\omega)\, e^{i\omega t}$ where the summation is over a discrete but infinite set of frequencies $\{\omega\}$ that are not necessarily equally or finitely spaced, since the motion may be

aperiodic. A continuous Fourier transform is not used because $\varepsilon_j(t)$ has a discrete spectrum of delta functions, excited by the continual rotation of the interacting pairs of rotors. The torque and noise functions are similarly expanded. Thus, mean values are given by $\hat{\varepsilon}_j(0) = 0$ and $\hat{\tau}_j(0) = \overline{\tau}$, and Eq. 3 becomes

$$-\omega^2\,\hat{\varepsilon}_j(\omega) = \hat{\tau}_{j+1}(\omega) + \hat{\tau}_{j-1}(\omega) - 2\hat{\tau}_j(\omega). \qquad (4)$$

Analysis is thus far exact. We now assume small fluctuations and linearize Eq. 2 with respect to ε_j, yielding [27] the torque-spectrum

$$\begin{aligned}\hat{\tau}_j(\omega) = \mu\, s_j\, \delta(\omega,0) + \tfrac{1}{2} i b_j^* \delta(\omega,-s_j) - \tfrac{1}{2} i b_j \delta(\omega,s_j) + \hat{\eta}_j(\omega) \\ + i\omega\mu\hat{\varepsilon}_j(\omega) + \tfrac{1}{2} b_j \hat{\varepsilon}_j(\omega - s_j) + \tfrac{1}{2} b_j^* \hat{\varepsilon}_j(\omega + s_j)\end{aligned} \qquad (5)$$

where $\hat{\eta}_j(\omega) \equiv \langle \eta_j(t)\, \exp(-i\omega t)\rangle$ and $b_j \equiv \exp(ic_j)$ and asterisks indicate complex-conjugation. In principal, solution of Eqs 4 and 5 gives the torque for any given configuration of shear rates $\{s_j\}$ and offsets $\{c_j\}$, thus yielding a spatial constitutive relation for the XY model. Torque uniformity then restricts the allowed configurations, yielding phase behaviour. The solution is straightforward in solid regions, where $s_j = 0$, and we find $\overline{\tau} = \sin(c_j)$, representing an elastic response to the mean angle of twist, c_j.

For general s_j we develop a mean-field theory, assuming uncorrelated fluctuations of neighbours. Averaging Eq. 4 over complex phase of $\hat{\tau}_{j+1}$ and $\hat{\tau}_{j+1}$, only their zero-frequency contributions remain, yielding

$$\omega^2\,\hat{\varepsilon}_j(\omega) = 2\hat{\tau}_j(\omega) - 2\overline{\tau}\,\delta(\omega,0), \qquad (6)$$

equivalent to placing a single rotor-pair in a medium of constant torque. In a fluid region, where $s_j \neq 0$, the offset c_j becomes arbitrary, so we then choose $c_j = 0$. Only one shear rate $s_j = s$ remains, so Eq. 5 and 6 generate harmonic spectra at integer multiples of s.

We make further progress, in the mean-field spirit, by dropping (average over) the noise term, equivalent to setting zero temperature and, without further approximation, obtain a recurrence relation for the ratio $R_n \equiv \hat{\varepsilon}_j(ns)/\hat{\varepsilon}_j([n-1]s)$ for $n > 1$: $1/R_n = ns(ns - 2i\mu) - R_{n+1}$. Using this to define the variable R_1 allows us to express a neat consititutive relation, involving the imaginary part of a continued fraction,

$$\begin{aligned}\overline{\tau} &= \sin(c_j)\,\delta(s,0) + \mu s + \Im(R_1) \qquad (7)\\ R_1 &= \cfrac{1}{s(s-2i\mu) - \cfrac{1}{2s(2s-2i\mu) - \cfrac{1}{3s(3s-2i\mu) - \frac{1}{\cdots}}}},\end{aligned}$$

plotted in Fig. 4a for various values of μ.

A local constitutive relation (a fluid's stress as a function of *local* shear rate, Fig. 4a), has a standard interpretation [29]. A negative gradient indicates an unstable regime where unbalanced stresses due to small nonuniformities act to enhance the perturbation. Coexistences

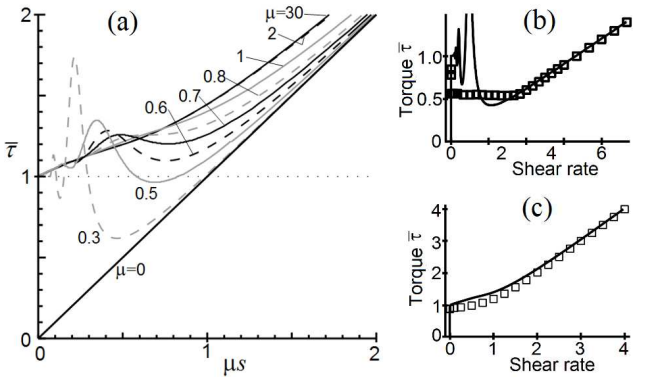

FIG. 4: (a) Mean-field predictions (Eq. 7) of torque $\overline{\tau}$ *versus* μs, where μ is friction coefficient and s local shear rate, for various μ. (b & c) Comparison between the theory (continuous curves), as a function of *local* shear rate s, and simulation measurements (symbols) plotted against *global* shear rate $\dot{\gamma}$ at $T = 0.01$. Both are evaluated for (b) $\mu = 0.2$ and (c) $\mu = 1.0$.

can occur between s values at equal $\overline{\tau}$. Thus, coexistence is necessary wherever the gradient is negative, and forbidden wherever s is single-valued as a function of $\overline{\tau}$.

For $s = 0$, Eq. 7 describes a solid capable of supporting any torque in the range $|\overline{\tau}| < 1$, implying a vertical line segment in Fig. 4a. So curves below the dotted line (where $\overline{\tau} = 1$) at finite s allow solid-fluid coexistence.

So the approximate theory reproduces the observed uniform states at high μ, a continuous transition (inflection in Fig. 4a) to shear-banding on decreasing μ, and first-order "freezing" (to solid-fluid or slip-plane states) at lower μ. Furthermore, Eq. 7 is quantitatively reasonable, compared with simulation measurements(Fig. 4b and c) of $\overline{\tau}$ *versus* $\dot{\gamma}$ (the volume-weighted mean of s). Metastability complicates the simulations at $T = 0$ so the coldest reliable results ($T = 0.01$) are compared with the zero-temperature theory. In Fig. 4b, the systems crosses a phase transition (gradient discontinuity) directly from uniformity at high $\dot{\gamma}$ to the slip-plane state at low $\dot{\gamma}$. A near-critical response (diverging $(\partial\dot{\gamma}/\partial\overline{\tau})_{T,\mu}$) is seen at low s in (Fig. 4c), where large fluctuations were observed.

It is remarkable how closely the angular-momentum-conserving 1D XY model mimics diverse soft matter. All fluids have a uniform-flow regime. Shear-banding is found in polymers [8, 9], colloids [10, 11] and various surfactant phases [12–14]. Slip-planes occur in surfactant cubic phases [26] and polymer melts [30, 31], and both slip and coexistences are seen in foams [15, 32] and colloids [10, 11, 33]. The existence of all four phenomena in a simple model with concise mean-field constitutive relation (Eq. 7) offers a paradigm for the physics underlying non-equilibrium complex fluids.

Acknowledgements We thank Adrian Baule for sage advice. Parts of this work were funded by a Royal Society University Research Fellowship, EPSRC grant GR/T24593/01, a Nuffield Foundation bursary URB/37198 and an EPSRC doctoral training grant.

[1] Kosterlitz and Thouless, Ordering, stability and phase transitions in two-dimensional systems. J Phys C **6**, 1181 (1973).

[2] J Toner and Y Tu, Long-range order in a two-dimensional dynamical XY model: how birds fly together. Phys. Rev. Lett. **75**, 4326 (1995).

[3] D. H. Lee and G. Grinstein, Strings in two-dimensional classical XY models. Phys. Rev. Lett. **55**, 541 (1985).

[4] H. G. Evertz and D. P. Landau, Critical dynamics in the two-dimensional classical XY model: A spin-dynamics study. Phys. Rev. B **54**, 12302 (1996).

[5] D. C. Mattis, Transfer matrix in plane-rotator model. Phys. Lett. A **104**, 357 (1984).

[6] Soft and Fragile Matter, M. E. Cates and M. R. Evans, eds. (IoP Publishing, Bristol, 1999).

[7] R. Jones, Soft Condensed Matter (Oxford 2002).

[8] J. Cao and A. E. Likhtman, Shear Banding in Molecular Dynamics of Polymer Melts. Phys. Rev. Lett. **108**, 028302 (2012).

[9] I. Kunita, K. Sato, Y. Tanaka, Y. Takikawa, H. Orihara, and T. Nakagaki, Shear Banding in an F-Actin Solution. Phys. Rev. Lett. **109**, 248303 (2012).

[10] R. Besseling, L. Isa, P. Ballesta, G. Petekidis, M. E. Cates, and W. C. K. Poon, Shear Banding and Flow-Concentration Coupling in Colloidal Glasses. Phys. Rev. Lett. **105**, 268301 (2010).

[11] F. Ianni, R. Di Leonardo, S. Gentilini, and G. Ruocco, Shear-banding phenomena and dynamical behavior in a Laponite suspension. Phys. Rev. E **77**, 031406 (2008).

[12] V. Schmitt, F. Lequeux, A. Pousse, and D. Roux. Flow behaviour and shear induced transition near an isotropic/nematic transition in equilibrium polymers. Langmuir **10**, 955 (1994).

[13] M. A. Fardin, D. Lopez, J. Croso, G. Grégoire, O. Cardoso, G. H. McKinley, and S. Lerouge, Elastic Turbulence in Shear Banding Wormlike Micelles. Phys. Rev. Lett. **104**, 178303 (2010).

[14] J.-B. Salmon, S. Manneville, and A. Colin, Shear banding in a lyotropic lamellar phase. I. Time-averaged velocity profiles. Phys. Rev. E **68**, 051503 (2003).

[15] K. Krishan and M. Dennin, Viscous shear banding in foam Phys. Rev. E **78**, 051504 (2008).

[16] J. M. Adams and P. D. Olmsted, Nonmonotonic Models are Not Necessary to Obtain Shear Banding Phenomena in Entangled Polymer Solutions Phys. Rev. Lett. **102**, 067801 (2009).

[17] S. M. Fielding and P. D. Olmsted, Spatiotemporal oscillations and rheochaos in a simple model of shear banding. Phys. Rev. Lett., **92**, 084502 (2004).

[18] J. K. G. Dhont, A constitutive relation describing the shear-banding transition. Phys. Rev. E **60**, 4534 (1999).

[19] J. M. Adams, S. M. Fielding and P. D. Olmsted, Transient shear banding in entangled polymers: A study using the Rolie-Poly model. J. Rheol. **55**, 1007 (2011).

[20] M. J. Unterberger, H. Weisbecker, G. A. Holzapfel, Mechanical modeling of rheometer experiments: Applications to rubber and actin networks. Int. J. Non-Linear Mech. **67**, 300 (2014).

[21] M. Harvey and T. A. Waigh, Optical coherence tomography velocimetry in controlled shear flow. Phys. Rev. E **83**, 031502 (2011).

[22] M. Tempel, G. Isenberg, and E. Sackmann, Temperature-induced sol-gel transition and microgel formation in -actinin cross-linked actin networks: A rheological study. Phys. Rev. E **54**, 1802 (1996).

[23] R. D. Groot and P. B. Warren, Dissipative particle dynamics: Bridging the gap between atomistic and mesoscopic simulation. J. Chem. Phys. **107**, 4423 (1997).

[24] Animations are available online at `https://sites.google.com/site/rmlevans/xy-model-animations`

[25] M. Büttiker, E. P. Harris, and R. Landauer, Thermal activation in extremely underdamped josephson-junction circuits. Phys. Rev. B **28**, 1268 (1983).

[26] J. L. Jones and T. C. B. McLeish, Rheological Response of Surfactant Cubic Phases. Langmuir **11**, 785 (1995).

[27] A full version of the calculation, together with more numerical data, will appear in a longer article.

[28] Suzanne M. Fielding, Complex dynamics of shear banded flows. Soft Matter **3**, 1262 (2007).

[29] P.D. Olmsted, Two-state shear diagrams for complex fluids in shear flow, Europhys. Lett. **48**, 339 (1999).

[30] P. Tapadia and S.-Q. Wang, Yieldlike constitutive transition in shear flow of entangled polymeric fluids. Phys. Rev. Lett. **91**, 198301 (2003).

[31] E. Pouyan Boukany, S.-Q. Wang, and X. Wang, Step shear of entangled linear polymer melts: new experimental evidence for elastic yielding, Macromolecules **42**, 6261 (2009).

[32] G. Debrégeas, H. Tabuteau, and J.-M. di Meglio, Deformation and flow of a two-dimensional foam under continuous shear, Phys. Rev. Lett. 87 (2001), 178305.

[33] M.D. Haw, Jamming, two-fluid behaviour and selffiltration in concentrated colloidal suspensions, Phys. Rev. Lett. 92 (2004), 185506.